Journal of Imaging Informatics in Medicine
https://doi.org/10.1007/s10278-025-01489-4

Prediction of Future Risk of Moderate to Severe Kidney Function Loss Using a Deep Learning Model–Enabled Chest Radiography

Kai-Chieh Chen[1] · Shang-Yang Lee[2] · Dung-Jang Tsai[2,3] · Kai-Hsiung Ko[4] · Yi-Chih Hsu[4] · Wei-Chou Chang[4] · Wen-Hui Fang[5] · Chin Lin[1,2,3,6] · Yu-Juei Hsu[7,8]

Received: 4 December 2024 / Revised: 20 February 2025 / Accepted: 19 March 2025

Abstract

Chronic kidney disease (CKD) remains a major public health concern, requiring better predictive models for early intervention. This study evaluates a deep learning model (DLM) that utilizes raw chest X-ray (CXR) data to predict moderate to severe kidney function decline. We analyzed data from 79,219 patients with an estimated Glomerular Filtration Rate (eGFR) between 65 and 120, segmented into development ($n = 37{,}983$), tuning ($n = 15{,}346$), internal validation ($n = 14{,}113$), and external validation ($n = 11{,}777$) sets. Our DLM, pretrained on CXR-report pairs, was fine-tuned with the development set. We retrospectively examined data spanning April 2011 to February 2022, with a 5-year maximum follow-up. Primary and secondary endpoints included CKD stage 3b progression, ESRD/dialysis, and mortality. The overall concordance index (*C*-index) values for the internal and external validation sets were 0.903 (95% CI, 0.885–0.922) and 0.851 (95% CI, 0.819–0.883), respectively. In these sets, the incidences of progression to CKD stage 3b at 5 years were 19.2% and 13.4% in the high-risk group, significantly higher than those in the median-risk (5.9% and 5.1%) and low-risk groups (0.9% and 0.9%), respectively. The sex, age, and eGFR-adjusted hazard ratios (HR) for the high-risk group compared to the low-risk group were 16.88 (95% CI, 10.84–26.28) and 7.77 (95% CI, 4.77–12.64), respectively. The high-risk group also exhibited higher probabilities of progressing to ESRD/dialysis or experiencing mortality compared to the low-risk group. Further analysis revealed that the high-risk group compared to the low/median-risk group had a higher prevalence of complications and abnormal blood/urine markers. Our findings demonstrate that a DLM utilizing CXR can effectively predict CKD stage 3b progression, offering a potential tool for early intervention in high-risk populations.

Keywords Deep learning · Chronic kidney disease · Chest x-ray · eGFR · Artificial intelligence · Opportunistic screening

✉ Chin Lin
xup6fup@mail.ndmctsgh.edu.tw

✉ Yu-Juei Hsu
yujuei@mail.ndmctsgh.edu.tw

[1] Graduate Institute of Life Sciences, National Defense Medical Center, No.161, Min-Chun E. Rd., Sec. 6, Neihu 114, Taipei, Taiwan, Republic of China

[2] Military Digital Medical Center, Tri-Service General Hospital, National Defense Medical Center, Taipei, Taiwan, Republic of China

[3] Medical Technology Education Center, School of Medicine, National Defense Medical Center, Taipei, Taiwan, Republic of China

[4] Department of Radiology, Tri-Service General Hospital, National Defense Medical Center, Taipei, Taiwan, Republic of China

[5] Department of Family and Community Medicine, Tri-Service General Hospital, National Defense Medical Center, Taipei, Taiwan, Republic of China

[6] School of Public Health, National Defense Medical Center, Taipei, Taiwan, Republic of China

[7] Department of Biochemistry, National Defense Medical Center, Taipei, Taiwan

[8] Division of Nephrology, Department of Internal Medicine, Tri-Service General Hospital, National Defense Medical Center, No 325, Cheng-Kung Rd., Sec. 2, Neihu 114, Taipei, Taiwan, Republic of China

Published online: 02 April 2025

Introduction

The global prevalence of chronic kidney disease (CKD) is 9.1%, and it is largely preventable and treatable, deserving increased attention in global health policy decision-making [1]. Once CKD progresses to an advanced stage, it inevitably leads to various complications, drastically reducing the quality of life [2]. Despite the existence of effective methods to prevent progression [3, 4], awareness among patients and medical service providers remains low [5]. Currently, the management of CKD primarily relies on albuminuria tests and estimated Glomerular Filtration Rate (eGFR), calculated from serum creatinine levels [6]. Albuminuria testing plays a crucial role in diagnosing early-stage CKD; however, its scarcity has resulted in significant underdiagnosis [7]. In patients with hypertension or diabetes, studies estimate that approximately two-thirds of those with albuminuria remain undetected due to a lack of testing, highlighting a major gap in CKD detection [8]. Nevertheless, screening the entire population for albuminuria may not be cost-effective [9, 10]. Therefore, there is a consensus to focus screening efforts on high-risk groups [11].

Numerous studies have employed combined risk predictors and typically relied on multi-variable models to forecast CKD progression [12]. However, these studies consistently emphasize the significance of eGFR and albuminuria tests [13], which poses a challenge when albuminuria tests are unavailable. Furthermore, additional blood and urine parameters played a pivotal role in powering these risk stratification calculators [12]. However, their frequent omissions in electronic health records (EHRs) often render these conventional clinical risk scores unusable [14]. In the absence of blood and urine information, CKD's most critical risk factors include a history of diabetes or cardiovascular diseases, and it has been recommended to systematically screen patients with these conditions [11]. However, these diseases also face underdiagnosis issues [15], and relying solely on medical history for risk stratification lacks accuracy in the context of CKD. There is a need to develop new risk stratification tools for early CKD to address the challenges faced by traditional EHR-based aggregate models when applied on a large scale.

A highly promising screening approach, known as opportunistic screening, has recently gained significant attention and application [16]. Traditionally, this method is performed by radiologists, such as when they identify potential osteoporosis patients while interpreting chest radiographs (CXR) [17]. The advent of deep learning models has prompted considerations for integrating artificial intelligence (AI) into radiological daily practices for such screening [18]. A recent randomized controlled trial has also demonstrated that AI-enabled CXR (AI-CXR) for opportunistic screening of osteoporosis has the potential to address the problem of underdiagnosis [19]. AI-CXR can be used not only to interpret osteoporosis but also to identify risk factors for early-stage CKD from chest X-rays, such as diabetes [20] and risk of cardiovascular diseases [21]. Therefore, we hypothesize that AI-CXR has the potential to serve as a risk stratification method for CKD. Considering that over 2 billion CXR are performed worldwide annually [22], an AI-CXR risk stratification tool that does not require data integration has the potential to identify patients with high risk of early-stage CKD, prompting early diagnosis and intervention for these patients. This study aimed to develop an AI model to identify high-risk groups for early-stage CKD, thereby offering a future opportunity to address the underdiagnosis of early-stage CKD.

Methods

Data Source and Population

This study received ethical approval from the Institutional Review Board (IRB NO. C202305019) at Tri-Service General Hospital in Taipei, Taiwan. Given the retrospective nature of the study, which involved anonymized and encrypted data, individual patient consent was not required. Data were collected from two facilities within the Tri-Service General Hospital system: an academic medical center in the Neihu District (Hospital A) and a community hospital in the Zhongzheng District (Hospital B), over a period spanning from April 2011 to February 2022. The research focused on patients who had estimated Glomerular filtration rate (eGFR) values recorded within 1 year prior to undergoing a chest X-ray (CXR). Our study included individuals with eGFR 60–120 ml/min/1.73m^2, spanning normal kidney function to mild CKD, ensuring a broad range of early CKD risk levels. All had at least one postero-anterior (PA) CXR with radiological labels, demographics, disease history, and lab results. Patients younger than 20 years were excluded from the analysis. To prevent potential CKD treatments from interfering with the model's predictive accuracy, patients who have previously been treated with angiotensin-converting enzyme inhibitors, angiotensin receptor blockers, pentoxifylline, dipyridamole, or sodium bicarbonate were excluded.

Our database comprised 79,219 patients for analysis, as shown in Fig. 1. Hospital A contributed 67,442 patients, each having undergone at least one CXR. To prevent overlap, each patient was assigned to only one dataset. Patients with multiple CXRs were allocated to the development set, while

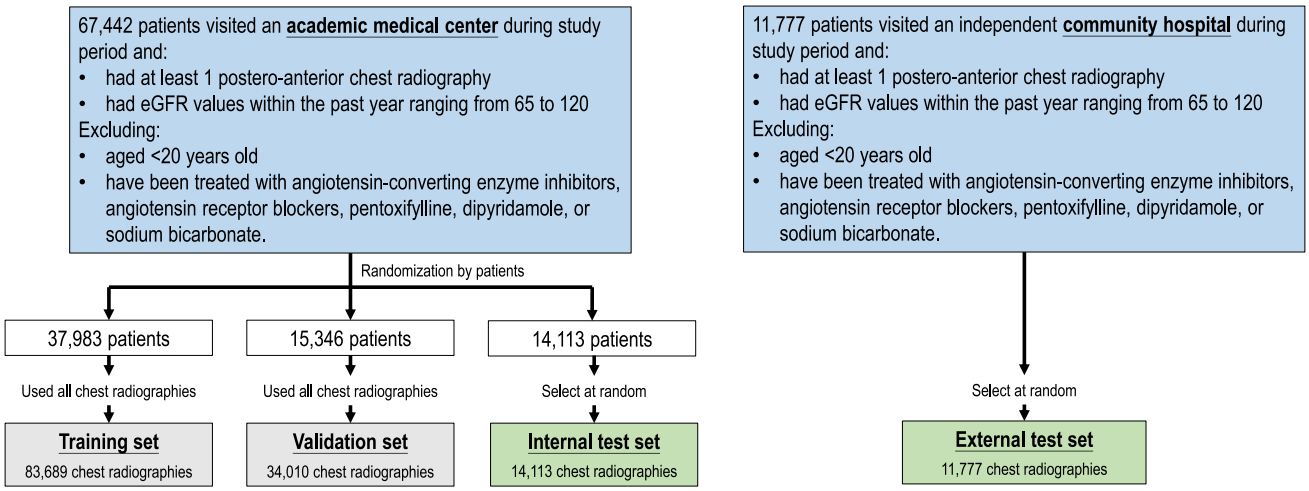

Fig. 1 Creation of development, tuning, internal validation, and external validation sets. This figure depicts the methodology employed for constructing and analyzing datasets to guarantee their durability and trustworthiness in training, validating, and testing the network. Each patient's data was segregated into distinct sets, ensuring the isolation of information and avoiding any potential "cross-contamination" between the training, validation, and test datasets

those with a single CXR were placed in the tuning, internal validation, or external validation sets. From Hospital A, 37,983 patients were included in the development set, contributing 83,689 CXRs for training our deep learning model (DLM). Additionally, 15,346 patients were assigned to the tuning set, providing 34,010 CXRs for refining the model. The internal validation set consisted of 14,113 independent patients, using only their initial CXR for evaluation. To evaluate the generalizability of our DLM, we incorporated data from Hospital B, involving 11,777 patients selected using the same criteria as those for the internal validation set to maintain consistency. To avoid over-representation of sicker patients who undergo frequent CXR examinations, we randomly sampled a single CXR per patient for each dataset. This method ensures a representation of diverse clinical scenarios, reflecting routine model deployment where CXRs are obtained at various stages of a patient's treatment course.

Patient Characteristics

Patient characteristics were extracted from the hospital information systems, with their pre-index medical histories identified through the International Classification of Diseases (ICD) codes. The conditions assessed included diabetes mellitus (DM, ICD-9 codes 250.x and ICD-10 codes E11.x), hypertension (HTN, ICD-9 codes 401.x to 404.x and ICD-10 codes I10.x to I16.x), hyperlipidemia (HLP, ICD-9 codes 272.x and ICD-10 codes E78.x), chronic kidney disease (CKD, ICD-9 codes 585.x and ICD-10 codes N18.x), heart failure (HF, ICD-9 codes 428.x, 398.91, and 402.$\times$1, and ICD-10 codes I50.x), coronary artery disease (CAD, ICD-9 codes 410.x to 414.x, and 429.2, and ICD-10 codes I20.x to I25.x), and chronic obstructive pulmonary disease (COPD, ICD-9 codes 490.x to 496.x and ICD-10 codes J44.9).

In our database, each CXR report includes 45 radiological labels, which were systematically extracted using a structured natural language processing-assisted approach and subsequently annotated and verified by a team of board-certified radiologists to ensure consistency and accuracy. These labels encompass a range of findings such as consolidation change, pneumonia, emphysematous change, pneumothorax, atelectasis, scalloping of the diaphragm, costophrenic angle blunting, pleural effusion, atherosclerosis, cardiomegaly, prominence of hilar shadow, pulmonary edema, aneurysm, degenerative joint disease, fracture, spondylosis, osteophyte formation, osteoporosis, osteoarthritis, widening of the mediastinum, malignancy, inflammatory, pigtail or drainage, sternotomy, port implantation, perm catheter insertion, pacemaker, tracheostomy, vertebroplasty, endotracheal tube, and nasogastric tube. These features are crucial for explaining the predictive basis of our AI-enhanced CXR analysis.

In addition to the eGFR, we collected key blood laboratory values from 1 year prior to the CXR, including blood urea nitrogen (BUN), urinary protein (uPro), microalbumin (mAlb), albumin-to-creatinine ratio (ACR), glucose (GLU), hemoglobin A1c (HbA1c), triglycerides (TG), total cholesterol (TC), low-density lipoprotein (LDL), high-density lipoprotein (HDL), and uric acid (UA).

Outcomes

In this study, the primary outcome was defined as having at least two eGFR values less than or equal to 45, indicative of

CKD stage 3b. We also defined two secondary outcomes: (1) end-stage renal disease (ESRD) or initiation of dialysis and (2) all-cause mortality. To minimize bias from incomplete records, data on patient visits were censored at the last known hospital encounter when the patient was alive. Additionally, the initiation of treatment with angiotensin-converting enzyme inhibitors, angiotensin receptor blockers, pentoxifylline, dipyridamole, or sodium bicarbonate was considered a censoring event to avoid interference from CKD treatment plans.

Implementation of the Deep Learning and Machine Learning Models

The CXR images in our study were stored in DICOM format with a resolution exceeding 2000 × 2000 pixels. Our primary feature extraction architecture was based on CheXzero [23], which integrates an image encoder and a language encoder pretrained on pairs of CXR images and associated radiological reports. We utilized the image encoder component, specifically a vision transformer (ViT-B/32), to extract embeddings for each CXR in our dataset. Each image was resized to a resolution of 256 × 256 to align with the network structure, followed by image normalization to ensure consistency across input images. The processed images were then encoded into a 512-dimensional feature vector. We applied the weight "best_64_0.0001_original_35000_0.864," which was the best publicly available model checkpoint from the original CheXzero study [23], selected based on its performance in prior evaluations. We used the pretrained model as a feature extractor without fine-tuning, as CheXzero has demonstrated strong generalization across multiple datasets. The extracted feature vectors were used to develop a Cox regression model to predict the development of CKD stage 3b, which we termed the CXR-risk score. The same model was also employed to predict progression to ESRD/dialysis and all-cause mortality without re-fitting by the Cox regression model. Risk stratification into low-, medium-, and high-risk groups was performed post-training, based on model-derived risk scores. Thresholds were optimized using the Youden index and *F*-score from the tuning set, ensuring effective classification for CKD progression. These processes were conducted within a Python environment, specifically version 3.10.10, using the "torch" package version 2.0.1.

We also conducted training using an XGBoost (eXtreme Gradient Boosting) classifier, employing the same datasets as those used in the DLM for predicting CKD stage 3b. This machine learning algorithm incorporated all available patient demographics and radiological labels. To ensure the model's robustness, 45 radiological features were evaluated based on correlation scores, and highly correlated features were excluded to prevent redundancy and minimize the influence of overlapping pathological conditions. The final model included the top eight most important features, selected for optimal predictive performance. The training was executed using the xgboost package version 0.71.2 in R, with default prediction parameters. Additionally, we utilized the XGBoost classifier to generate new predictions by integrating outputs from the DLM with patient characteristics. These predictions were subsequently used to evaluate and compare the accuracy levels achieved by both methodologies.

Statistical Analysis

The characteristics of the different datasets are presented using descriptive statistics, including means, standard deviations, patient counts, and percentages. Continuous variables were analyzed using either Student's *t*-test or analysis of variance, and results are presented as mean ± SD. Categorical variables were assessed using the $\chi 2$ test or Fisher's exact test, depending on appropriateness. The performance of the deep learning model (DLM) was evaluated through Kaplan–Meier survival curves for predicting the development of CKD stage 3b and other secondary outcomes, with the concordance index (*C*-index) calculated to assess model accuracy. The operational thresholds for median risk and high risk were set based on the incidence of CKD stage 3b within a 5-year period, utilizing the maximum Youden's index and *F*-score from the tuning set. Statistical analyses were performed using R version 3.4.4. For multiple comparisons, Bonferroni correction was applied to adjust the significance threshold.

Results

Baseline Characteristics

The patient characteristics of the development, tuning, internal validation, and external validation sets are summarized in Table 1, with all variables showing differences across datasets. In the development set, the average eGFR was 96.2 ± 13.6, which included 12,136 patients (32.0%) with eGFR below 90 ml/min, 15,751 patients (41.5%) with eGFR between 90 and 105 ml/min, and 10,096 patients (26.6%) with eGFR between 106 and 120 ml/min. In the internal validation set, the average eGFR was 96.4 ± 13.3, with 4391 patients (31.1%) below 90 ml/min, 6030 patients (42.7%) between 90 and 105 ml/min, and 3692 patients (26.2%) between 106 and 120 ml/min. Similarly, in the external validation set, the average eGFR was 95.6 ± 13.2, with 3927 patients (33.3%) below 90 ml/min, 5067 patients (43.0%) between 90 and 105 ml/min, and 2783 patients (23.6%) between 106 and 120 ml/min. Additionally, Extended Data

Table 1 Baseline characteristics

Variable	Development set (n = 37,983)	Tuning set (n = 15,346)	Internal validation set (n = 14,113)	External validation set (n = 11,777)	p value
eGFR	96.2 ± 13.6	96.2 ± 13.5	96.4 ± 13.3	95.6 ± 13.2	< 0.001†
eGFR group					< 0.001†
< 90 ml/min	12,136 (32.0%)	4966 (32.4%)	4391 (31.1%)	3927 (33.3%)	
90–105 ml/min	15,751 (41.5%)	6335 (41.3%)	6030 (42.7%)	5067 (43.0%)	
106–120 ml/min	10,096 (26.6%)	4045 (26.4%)	3692 (26.2%)	2783 (23.6%)	
Demographics					
Age	52.3 ± 15.6	52.3 ± 15.6	51.4 ± 15.1	52.6 ± 15.7	< 0.001†
Age group					< 0.001†
< 50 y/o	16,320 (43.0%)	6684 (43.6%)	6325 (44.8%)	4917 (41.8%)	
50–59 y/o	8936 (23.5%)	3573 (23.3%)	3451 (24.5%)	2684 (22.8%)	
60–69 y/o	8083 (21.3%)	3174 (20.7%)	2936 (20.8%)	2747 (23.3%)	
> 69 y/o	4644 (12.2%)	1915 (12.5%)	1401 (9.9%)	1429 (12.1%)	
Gender					< 0.001†
Female	19,183 (50.5%)	7779 (50.7%)	7407 (52.5%)	6389 (54.2%)	
Male	18,800 (49.5%)	7567 (49.3%)	6706 (47.5%)	5388 (45.8%)	
Data source					< 0.001†
ED	10,872 (28.6%)	4456 (29.0%)	4000 (28.3%)	2976 (25.3%)	
IPD	10,114 (26.6%)	4068 (26.5%)	3740 (26.5%)	2874 (24.4%)	
OPD	16,997 (44.7%)	6822 (44.5%)	6373 (45.2%)	5927 (50.3%)	
Image technology					< 0.001†
CR	8043 (21.2%)	3208 (20.9%)	2963 (21.0%)	1994 (16.9%)	
DX	29,940 (78.8%)	12,138 (79.1%)	11,150 (79.0%)	9783 (83.1%)	
Disease histories					
DM	3121 (8.2%)	1270 (8.3%)	973 (6.9%)	1338 (11.4%)	< 0.001†
HTN	584 (1.5%)	244 (1.6%)	160 (1.1%)	284 (2.4%)	< 0.001†
HLP	6577 (17.3%)	2600 (16.9%)	2173 (15.4%)	3406 (28.9%)	< 0.001†
HF	424 (1.1%)	185 (1.2%)	88 (0.6%)	124 (1.1%)	< 0.001†
CAD	2925 (7.7%)	1208 (7.9%)	907 (6.4%)	1187 (10.1%)	< 0.001†
COPD	3189 (8.4%)	1241 (8.1%)	788 (5.6%)	1355 (11.5%)	< 0.001†

ED emergency department, *IPD* inpatient department, *OPD* outpatient department, *CR* computed radiography, *DX* digital radiography, *DM* diabetes mellitus, *HTN* hypertension, *HLP* hyperlipidemia, *HF* heart failure, *CAD* coronary artery disease, *COPD* chronic obstructive pulmonary disease

†Adjusted significance level (α) = 0.00384, indicating statistical significance

Table 1 and Extended Data Table 2 describe the demographic and radiological disease distributions of patients stratified by CKD 3B status at the 5-year follow-up.

Prediction of Long-Term Risk of Developing CKD Stage 3b, ESRD/Dialysis, and Mortality Events

Using the tuning set, patients were stratified into low, median, and high-risk groups based on cutoff points determined by maximum Youden's index and F-scores. Figure 2 illustrates the progression to CKD stage 3b, progression to ESRD/dialysis, and mortality rates across these risk categories. In the internal validation set, the incidences of progression to CKD stage 3b were 9.1% at 2 years and 19.2% at 5 years in the high-risk group, significantly higher than those in the median-risk group (1.4% at 2 years and 5.9% at 5 years) and low-risk group (0.1% at 2 years and 0.9% at 5 years). The sex, age, and eGFR-adjusted hazard ratio (HR) for this group was 16.88 (95% CI, 10.84–26.28). Similarly, the incidences of progression to ESRD/dialysis were 2.4% at 2 years and 4.7% at 5 years in the high-risk group, significantly higher than in the median-risk group (0.4% at 2 years and 1.6% at 5 years) and low-risk group (0.0% at 2 years and 0.1% at 5 years), with a corresponding HR of 73.44 (95% CI, 23.62–228.36). Additionally, the incidences of all-cause mortality were 8.9% at 2 years and 15.2% at 5 years in the high-risk group, markedly higher than those in the median-risk group (2.5%

Table 2 Demographic characteristics in internal and external validation set

Variable	Internal validation				External validation			
	Low risk (n = 11,653)	Median risk (n = 1372)	High risk (n = 1088)	p value*	Low risk (n = 9851)	Median risk (n = 1090)	High risk (n = 836)	p value*
eGFR	98.0 ± 13.0	89.5 ± 12.1	88.0 ± 12.2	< 0.001†	97.2 ± 12.9	88.2 ± 11.7	86.3 ± 11.7	< 0.001†
eGFR group				< 0.001†				< 0.001†
65–90 ml/min	3066 (26.3%)	693 (50.5%)	632 (58.1%)		2772 (28.1%)	619 (56.8%)	536 (64.1%)	
90–105 ml/min	5111 (43.9%)	558 (40.7%)	361 (33.2%)		4420 (44.9%)	400 (36.7%)	247 (29.5%)	
106–120 ml/min	3476 (29.8%)	121 (8.8%)	95 (8.7%)		2659 (27.0%)	71 (6.5%)	53 (6.3%)	
Demographics								
Age	48.0 ± 13.5	64.2 ± 10.6	71.4 ± 11.4	< 0.001†	49.2 ± 14.1	66.4 ± 10.5	73.6 ± 11.9	< 0.001†
Age group				< 0.001†				< 0.001†
< 50 y/o	6163 (52.9%)	125 (9.1%)	37 (3.4%)		4810 (48.8%)	82 (7.5%)	25 (3.0%)	
50–59 y/o	2999 (25.7%)	302 (22.0%)	150 (13.8%)		2404 (24.4%)	191 (17.5%)	89 (10.6%)	
60–69 y/o	2061 (17.7%)	564 (41.1%)	311 (28.6%)		2126 (21.6%)	405 (37.2%)	216 (25.8%)	
> 69 y/o	430 (3.7%)	381 (27.8%)	590 (54.2%)		511 (5.2%)	412 (37.8%)	506 (60.5%)	
Gender				< 0.001†				< 0.001†
Female	6303 (54.1%)	592 (43.1%)	512 (47.1%)		5439 (55.2%)	556 (51.0%)	394 (47.1%)	
Male	5350 (45.9%)	780 (56.9%)	576 (52.9%)		4412 (44.8%)	534 (49.0%)	442 (52.9%)	
Data source				< 0.001†				< 0.001†
ED	3120 (26.8%)	508 (37.0%)	372 (34.2%)		2471 (25.1%)	280 (25.7%)	225 (26.9%)	
IPD	2804 (24.1%)	474 (34.5%)	462 (42.5%)		2207 (22.4%)	331 (30.4%)	336 (40.2%)	
OPD	5729 (49.2%)	390 (28.4%)	254 (23.3%)		5173 (52.5%)	479 (43.9%)	275 (32.9%)	
Image technology				< 0.001†				0.028
CR	2626 (22.5%)	185 (13.5%)	152 (14.0%)		1689 (17.1%)	154 (14.1%)	151 (18.1%)	
DX	9027 (77.5%)	1187 (86.5%)	936 (86.0%)		8162 (82.9%)	936 (85.9%)	685 (81.9%)	
Disease histories								
DM	654 (5.6%)	169 (12.3%)	150 (13.8%)	< 0.001†	962 (9.8%)	224 (20.6%)	152 (18.2%)	< 0.001†
HTN	128 (1.1%)	19 (1.4%)	13 (1.2%)	0.626	208 (2.1%)	47 (4.3%)	29 (3.5%)	< 0.001†
HLP	1767 (15.2%)	242 (17.6%)	164 (15.1%)	0.053	2805 (28.5%)	389 (35.7%)	212 (25.4%)	< 0.001†
HF	32 (0.3%)	16 (1.2%)	40 (3.7%)	< 0.001†	52 (0.5%)	30 (2.8%)	42 (5.0%)	< 0.001†
CAD	666 (5.7%)	136 (9.9%)	105 (9.7%)	< 0.001†	889 (9.0%)	164 (15.0%)	134 (16.0%)	< 0.001†
COPD	582 (5.0%)	97 (7.1%)	109 (10.0%)	< 0.001†	1022 (10.4%)	173 (15.9%)	160 (19.1%)	< 0.001†

ED emergency department, *IPD* inpatient department, *OPD* outpatient department, *CR* computed radiography, *DX* digital radiography, *DM* diabetes mellitus, *HTN* hypertension, *HLP* hyperlipidemia, *HF* heart failure, *CAD* coronary artery disease, *COPD* chronic obstructive pulmonary disease

*Hypothesis test of the difference between the low risk, median risk, and high risk

†Adjusted significance level (α) = 0.00384, indicating statistical significance

at 2 years and 4.9% at 5 years) and low-risk group (0.3% at 2 years and 0.7% at 5 years), with an HR of 22.53 (95% CI, 14.58–34.80). A clear dose–response relationship was evident, with HRs increasing from the low to the high-risk group. This relationship was also validated in the external validation set, underscoring the significant prognostic value of AI-enhanced CXR in predicting future progression to CKD stage 3b, ESRD/dialysis, and mortality.

Components of AI-CXR in Predicting CKD 3b Progression

To evaluate the efficacy of our DLM utilizing raw CXR data against traditional feature-based machine learning models (MLMs) for predicting future progression to CKD stage 3b, we conducted a comparative analysis. Based on the correlation matrix of 45 variables, highly correlated

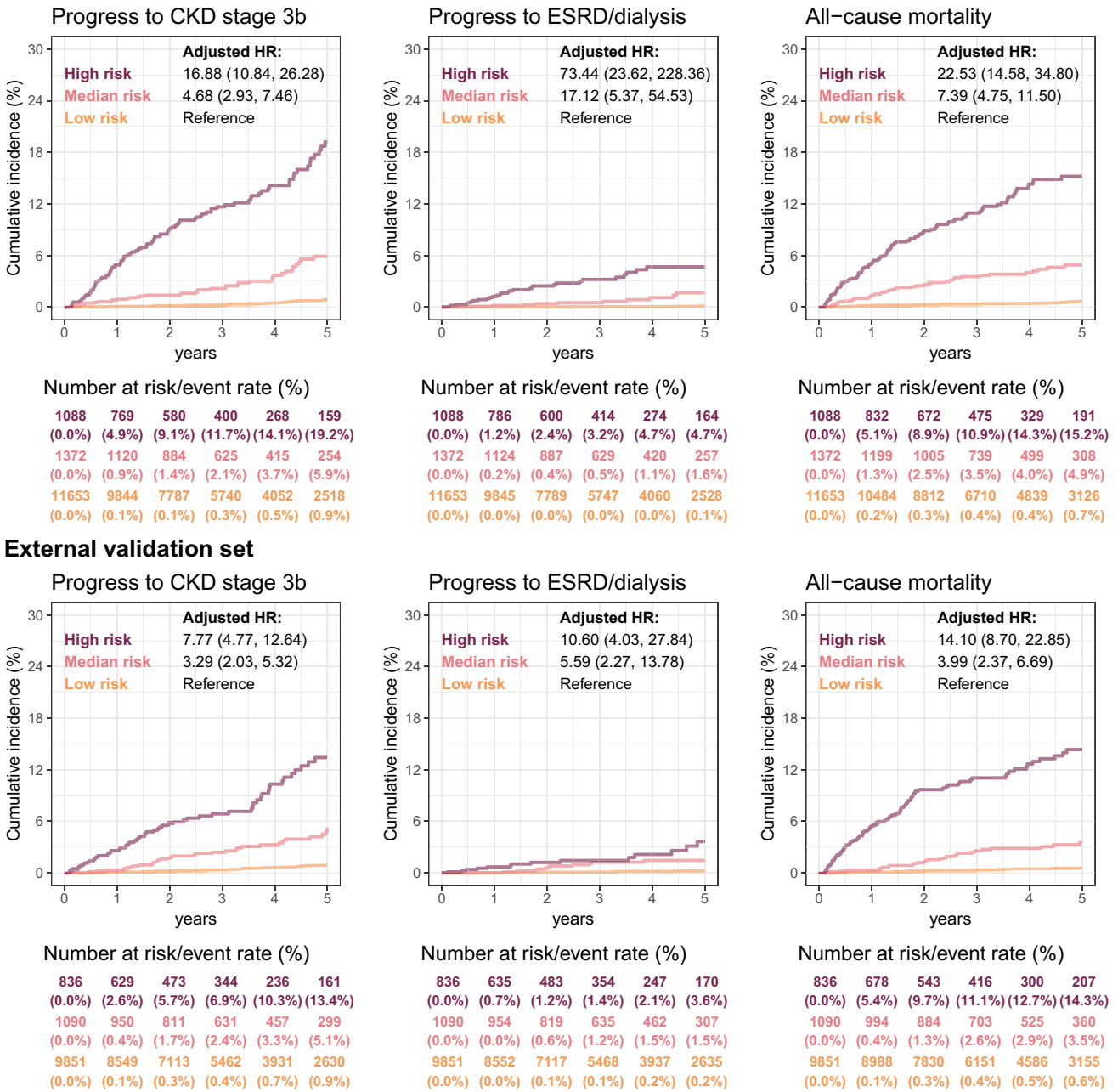

Fig. 2 Long-term incidence of developing CKD stage 3b, ESRD/dialysis, and mortality events stratified by AI-CXR. The analyses are performed on both internal and external validation sets. The table displays the population at risk and cumulative risk for specific time intervals in each risk stratification. It also includes the adjusted hazard ratio (adjusted gender, age, and eGFR) for comparison

variables were selectively retained to avoid redundancy, as detailed in Extended Data Fig. 1. Figure 3A details the composition of these MLMs, emphasizing patient characteristics such as age and eGFR as critical factors. Notably, atherosclerosis was identified as the most significant radiological characteristic in the models. Figure 3B presents the comparison of the concordance index (*C*-index) values derived from these parameters, MLMs, and the DLM. Extended Data Table 3 further presents a detailed performance comparison between the DLM and MLMs, highlighting key evaluation metrics. Remarkably, our DLM, which leverages raw CXR data, demonstrated superior performance compared to MLMs that rely on extracted radiological characteristics.

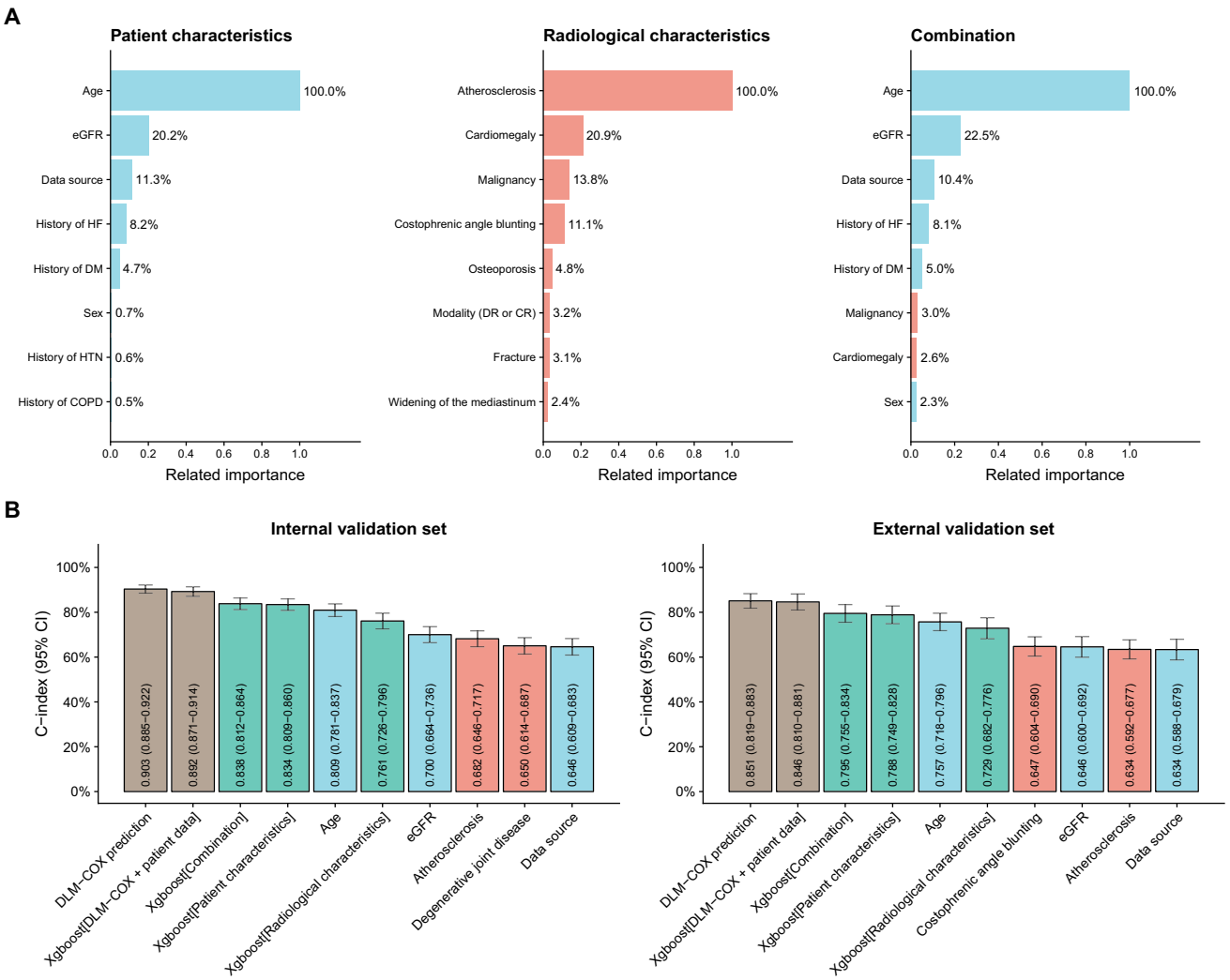

Fig. 3 A comparative analysisof AI-CXR and all available data. In **A**, we delineate the constituent components of conventional machine learning models utilized for this purpose. Specifically, we trained three xgboost models: one leveraging patient characteristics, another incorporating radiological characteristics, and the third amalgamating both datasets. Patient characteristics are depicted by the sky-blue bars, while radiological characteristics are represented by the orange bars. Transitioning to **B**, we present the C-index derived from all available eGFR-related data. This encompasses the performance of DLM-COX utilizing CXR data exclusively, as well as those integrating CXR data with patient characteristics. The sky-blue and orange bars denote the predictive outcomes based on individual patient characteristics and radiological characteristics, respectively. The green bars illustrate predictions integrating features extracted through xgboost, while the brown bars demonstrate predictions incorporating insights from DLM-COX. Each *C*-index is accompanied by error bars denoting the 95% confidence intervals (CI) for clarity and precision in estimation

Risk Features of Patients with Different Risks Identified by AI-CXR

In the internal validation set, the eGFR values for the high-risk group averaged 88.0 ± 12.2, which was significantly lower than those for the median risk (89.5 ± 12.1) and low-risk groups (98.0 ± 13.0). A clear dose–response relationship was evident, with eGFR decreasing progressively from the median/low-risk group to the high-risk group. Additionally, compared to the median/low-risk group, the high-risk group exhibited significantly older age, a higher prevalence of male gender, more inpatient department visits, utilization of digital radiography, and higher incidence of comorbidities such as DM, HF, CAD, and COPD. These trends were similarly observed in the external validation set, as depicted in Table 2.

Furthermore, in terms of radiological findings, the high-risk group demonstrated a significantly higher prevalence of radiological characteristics compared to the median/low-risk group, particularly for costophrenic angle blunting, pleural effusion, atherosclerosis, cardiomegaly, prominence of hilar shadow, and inflammatory, with similar trends noted in the

Table 3 Radiological characteristics in internal and external validation set

Variable	Internal validation				External validation			
	Low risk (n = 11,653)	Median risk (n = 1372)	High risk (n = 1088)	p value*	Low risk (n = 9851)	Median risk (n = 1090)	High risk (n = 836)	p value*
Consolidation change	61 (0.5%)	29 (2.1%)	80 (7.4%)	< 0.001†	59 (0.6%)	19 (1.7%)	53 (6.3%)	< 0.001†
Pneumonia	15 (0.1%)	9 (0.7%)	26 (2.4%)	< 0.001#†	10 (0.1%)	3 (0.3%)	10 (1.2%)	< 0.001#†
Emphysematous change	46 (0.4%)	24 (1.7%)	35 (3.2%)	< 0.001†	50 (0.5%)	24 (2.2%)	26 (3.1%)	< 0.001†
Pneumothorax	9 (0.1%)	12 (0.9%)	17 (1.6%)	< 0.001#†	18 (0.2%)	4 (0.4%)	18 (2.2%)	< 0.001#†
Atelectasis	23 (0.2%)	19 (1.4%)	38 (3.5%)	< 0.001†	19 (0.2%)	18 (1.7%)	34 (4.1%)	< 0.001†
Scalloping of the diaphragm	140 (1.2%)	42 (3.1%)	39 (3.6%)	< 0.001†	119 (1.2%)	53 (4.9%)	38 (4.5%)	< 0.001†
Costophrenic angle blunting	1229 (10.5%)	421 (30.7%)	596 (54.8%)	< 0.001†	1158 (11.8%)	367 (33.7%)	487 (58.3%)	< 0.001†
Pleural effusion	365 (3.1%)	148 (10.8%)	307 (28.2%)	< 0.001†	359 (3.6%)	125 (11.5%)	213 (25.5%)	< 0.001†
Atherosclerosis	2472 (21.2%)	863 (62.9%)	834 (76.7%)	< 0.001†	2380 (24.2%)	771 (70.7%)	669 (80.0%)	< 0.001†
Cardiomegaly	532 (4.6%)	343 (25.0%)	437 (40.2%)	< 0.001†	425 (4.3%)	252 (23.1%)	343 (41.0%)	< 0.001†
Prominence of hilar shadow	267 (2.3%)	108 (7.9%)	187 (17.2%)	< 0.001†	178 (1.8%)	95 (8.7%)	151 (18.1%)	< 0.001†
Pulmonary edema	6 (0.1%)	8 (0.6%)	25 (2.3%)	< 0.001#†	4 (0.0%)	9 (0.8%)	17 (2.0%)	< 0.001#†
Aneurysm	1 (0.0%)	0 (0.0%)	2 (0.2%)	0.020#	0 (0.0%)	1 (0.1%)	0 (0.0%)	0.164#
Degenerative joint disease	2668 (22.9%)	812 (59.2%)	728 (66.9%)	< 0.001†	2461 (25.0%)	688 (63.1%)	598 (71.5%)	< 0.001†
Fracture	267 (2.3%)	111 (8.1%)	150 (13.8%)	< 0.001†	246 (2.5%)	101 (9.3%)	128 (15.3%)	< 0.001†
Spondylosis	1170 (10.0%)	437 (31.9%)	477 (43.8%)	< 0.001†	1090 (11.1%)	385 (35.3%)	383 (45.8%)	< 0.001†
Osteophyte formation	2072 (17.8%)	679 (49.5%)	628 (57.7%)	< 0.001†	1950 (19.8%)	560 (51.4%)	523 (62.6%)	< 0.001†
Osteoporosis	276 (2.4%)	138 (10.1%)	173 (15.9%)	< 0.001†	323 (3.3%)	128 (11.7%)	137 (16.4%)	< 0.001†
Osteoarthritis	764 (6.6%)	321 (23.4%)	360 (33.1%)	< 0.001†	696 (7.1%)	278 (25.5%)	287 (34.3%)	< 0.001†
Widening of the mediastinum	412 (3.5%)	160 (11.7%)	247 (22.7%)	< 0.001†	374 (3.8%)	131 (12.0%)	201 (24.0%)	< 0.001†
Malignancy	20 (0.2%)	16 (1.2%)	47 (4.3%)	< 0.001†	17 (0.2%)	9 (0.8%)	27 (3.2%)	< 0.001#†
Inflammatory	710 (6.1%)	252 (18.4%)	393 (36.1%)	< 0.001†	688 (7.0%)	216 (19.8%)	312 (37.3%)	< 0.001†

*Hypothesis test of the difference between the low risk, median risk, and high risk

#p value calculated with $n < 25$ in continuous variables or by Fisher's exact test for categorical variables

†Adjusted significance level (α) = 0.00179, indicating statistical significance

external validation set, as outlined in Table 3. Regarding laboratory examinations, the high-risk group exhibited significantly elevated levels of BUN, GLU, and HbA1, along with a greater prevalence of ACR values ≥ 300 ug/mg. These trends were also observed in the external validation set, as detailed in Table 4.

Stratified Analysis of AI-CXR in Predicting CKD 3b Progression

We evaluated our model's performance across various subgroups, including CXR photography technique, data source, eGFR group, gender, age group, and comorbidities. The overall concordance indices (C-index) were 0.903 for the internal validation set and 0.851 for the external validation set. Notably, when assessing the impact of gender and age concurrently, we observed a decline in the C-index with increasing age. Specifically, among females under 50 years old, the highest C-index of 0.960 was recorded in the internal validation set, whereas the highest C-index for males under 50 years old in the external validation set was 0.865. Additionally, patients without comorbidities consistently exhibited higher C-index values, as depicted in Fig. 4.

Table 4 Laboratory characteristics in internal and external validation set

Variable	Internal validation				External validation			
	Low risk (n = 11,653)	Median risk (n = 1372)	High risk (n = 1088)	p value*	Low risk (n = 9851)	Median risk (n = 1090)	High risk (n = 836)	p value*
BUN	13.7 ± 4.0	15.8 ± 6.0	16.4 ± 6.4	< 0.001†	13.9 ± 4.1	15.5 ± 5.4	15.6 ± 5.9	< 0.001†
BUN group				< 0.001†				< 0.001†
BUN ≤ 20 mg/dl	8315 (94.8%)	873 (84.3%)	739 (79.8%)		6489 (94.2%)	688 (87.3%)	571 (84.1%)	
BUN > 20 mg/dl	456 (5.2%)	162 (15.7%)	187 (20.2%)		400 (5.8%)	100 (12.7%)	108 (15.9%)	
uPro	43.9 ± 178.6	22.5 ± 26.6	51.5 ± 184.6	0.656	19.7 ± 57.3	45.6 ± 145.0	36.3 ± 62.2	0.045
uPro group				0.525#				0.154#
uPro < 150 mg/dl	229 (95.8%)	44 (100.0%)	73 (96.1%)		288 (97.3%)	36 (94.7%)	52 (92.9%)	
uPro ≥ 150 mg/dl	10 (4.2%)	0 (0.0%)	3 (3.9%)		8 (2.7%)	2 (5.3%)	4 (7.1%)	
mAlb	8.8 ± 59.0	6.0 ± 15.2	13.4 ± 29.9	0.786	7.0 ± 52.6	5.7 ± 11.5	4.3 ± 7.5	0.908
mAlb group				0.053#				0.327#
mAlb < 30 mg/dl	324 (96.4%)	66 (94.3%)	32 (86.5%)		492 (97.2%)	96 (94.1%)	49 (98.0%)	
mAlb 30–299 mg/dl	10 (3.0%)	4 (5.7%)	5 (13.5%)		12 (2.4%)	6 (5.9%)	1 (2.0%)	
mAlb ≥ 300 mg/dl	2 (0.6%)	0 (0.0%)	0 (0.0%)		2 (0.4%)	0 (0.0%)	0 (0.0%)	
ACR	80.8 ± 476.7	46.5 ± 94.5	221.1 ± 379.7	0.160	69.1 ± 433.4	37.2 ± 62.2	52.9 ± 99.0	0.804
ACR group				< 0.001#†				< 0.001#†
ACR < 30 ug/mg	207 (79.6%)	45 (78.9%)	15 (46.9%)		326 (85.1%)	47 (67.1%)	25 (67.6%)	
ACR 30–299 ug/mg	44 (16.9%)	9 (15.8%)	10 (31.2%)		45 (11.7%)	22 (31.4%)	10 (27.0%)	
ACR ≥ 300 ug/mg	9 (3.5%)	3 (5.3%)	7 (21.9%)		12 (3.1%)	1 (1.4%)	2 (5.4%)	
GLU	98.9 ± 24.9	114.1 ± 38.4	118.5 ± 49.1	< 0.001†	102.3 ± 28.5	115.5 ± 35.5	110.3 ± 33.8	< 0.001†
GLU group				< 0.001†				< 0.001†
GLU < 100 mg/dl	3831 (70.8%)	194 (42.2%)	125 (42.8%)		3010 (62.7%)	193 (35.9%)	143 (45.0%)	
GLU 100–125 mg/dl	1226 (22.6%)	169 (36.7%)	90 (30.8%)		1344 (28.0%)	223 (41.4%)	121 (38.1%)	
GLU ≥ 126 mg/dl	357 (6.6%)	97 (21.1%)	77 (26.4%)		449 (9.3%)	122 (22.7%)	54 (17.0%)	
HbA1c	6.3 ± 1.6	6.9 ± 2.0	6.8 ± 1.7	< 0.001†	6.3 ± 1.6	6.8 ± 1.7	6.4 ± 1.1	< 0.001†
HbA1c group				< 0.001†				< 0.001†
HbA1c < 6.5%	1178 (75.7%)	189 (59.1%)	143 (55.6%)		1368 (72.8%)	184 (55.8%)	145 (62.8%)	
HbA1c 6.5–7.9%	228 (14.7%)	70 (21.9%)	72 (28.0%)		335 (17.8%)	88 (26.7%)	64 (27.7%)	
HbA1c ≥ 8.0%	150 (9.6%)	61 (19.1%)	42 (16.3%)		175 (9.3%)	58 (17.6%)	22 (9.5%)	

BUN blood urea nitrogen, *uPro* urinary protein, *mAlb* microalbumin, *ACR* albumin-to-creatinine ratio, *GLU* glucose, *HbA1c* hemoglobin A1c

*Hypothesis test of the difference between the low risk, median risk, and high risk

#p value calculated with $n < 25$ in continuous variables or by Fisher's exact test for categorical variables

†Adjusted significance level (α) = 0.00417, indicating statistical significance

Discussion

In this study, we developed and validated an AI model to predict the long-term risk of CKD progression risk using CXR. Our findings demonstrate that the AI model can stratify patients effectively into low-, median-, and high-risk groups with significant predictive value for CKD stage 3b, ESRD/dialysis, and all-cause mortality, as evidenced by robust concordance indices in both internal and external validation sets. Importantly, our AI model utilizing CXR alone outperformed traditional feature-based machine learning models, highlighting the potential advantages of

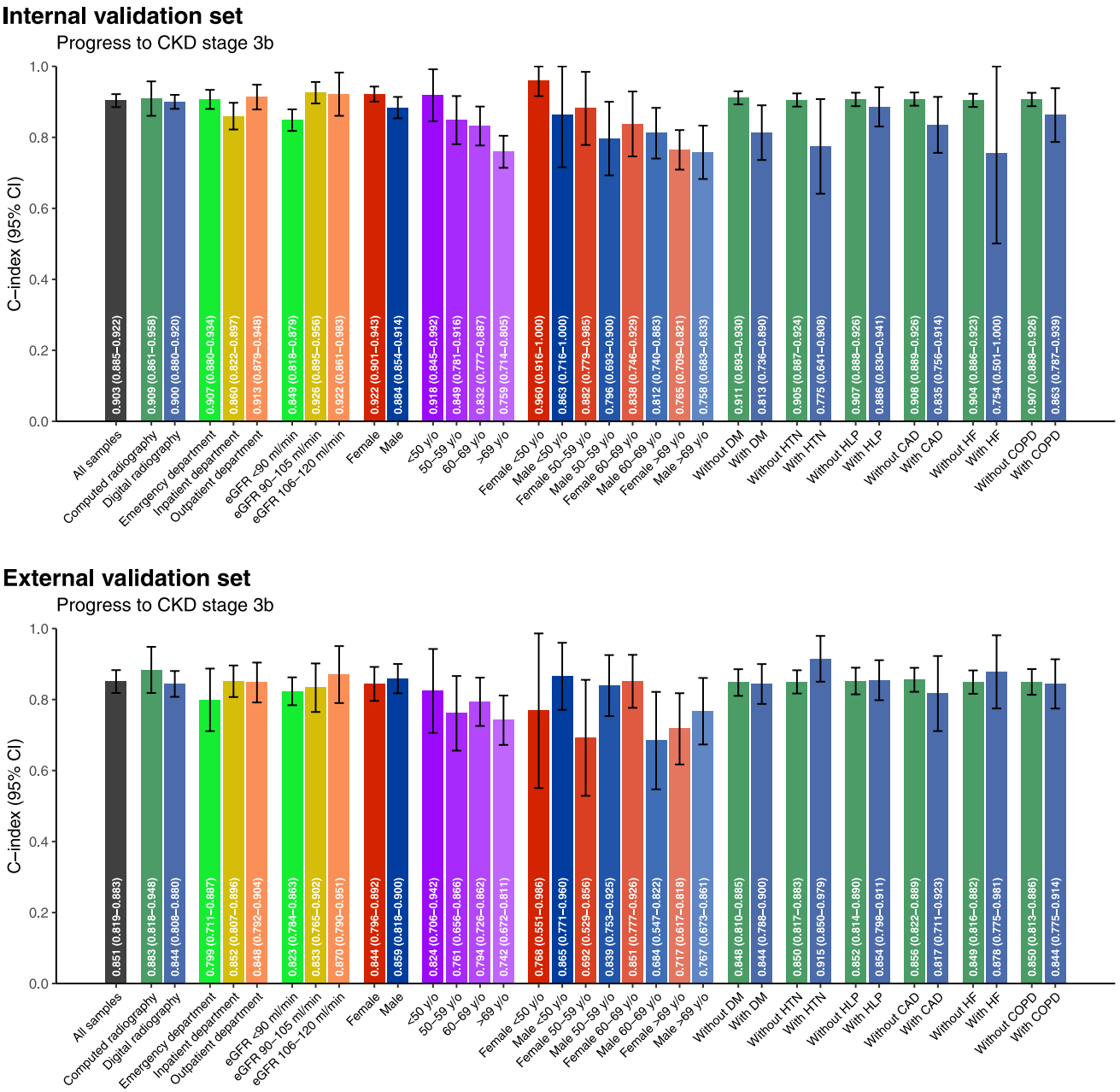

Fig. 4 Stratified analysis of selected patient characteristics to assess the performance of AI-CXR in predicting progress to CKD stage 3b. Bar charts with error bars representing the *C*-index and 95% confidence intervals (CI) depict the performance metrics. The analysis is categorized by several factors, including image technology (represented by forest green and ocean blue for computed radiography and digital radiography), data source (color-coded as light green, yellow–brown, and light orange for emergency department, inpatient department, and outpatient department), eGFR group (color-coded as light green, yellow–brown, and light orange for eGFR < 90 ml/min, eGFR 90–105 ml/min, and eGFR 106–120 ml/min), sex (highlighted in red and blue for female and male), and age (illustrated with shades of purple from dark to light to represent younger to older age groups), as well as comorbidities such as DM, HTN, HLP, CAD, HF, and COPD (indicated by forest green and ocean blue for without and with comorbidity). The performance results are presented for both the internal test set and the community test set, respectively

an AI-driven approach in leveraging complex imaging data for clinical prediction. These results suggest that AI-CXR may offer a valuable, cost-effective method for proactive CKD management.

Our study demonstrates that a single CXR can accurately predict CKD progression and even mortality, with consistent results across stratified analyses. It is reasonable that CXRs could reveal these risks, as many AI-CXR models

have already shown superior capabilities to human interpretation in identifying complex patterns linked to systemic disease. For example, AI-CXR models have outperformed clinicians in detecting osteoporosis [18], classifying cardiac functions [24], and predicting future major adverse cardiovascular events [21]—underscoring the untapped potential of radiographic data in forecasting health outcomes. Prior studies have also demonstrated the ability of CXRs to predict mortality [25, 26], supporting the idea that this imaging modality can provide valuable prognostic information beyond its immediate clinical purpose. However, there are limited prior research on the use of CXRs to predict CKD specifically, though studies employing AI-enabled electrocardiogram for CKD prediction underscore the viability of imaging-based approaches for renal risk stratification [27]. Given this context, our model's performance supports its reliability and potential utility as a novel tool for early CKD risk identification, meriting further exploration in clinical practice.

The predictive capabilities of AI-CXR in assessing CKD progression are strongly associated with traditional CKD risk factors. In our study, the incidence of comorbidities and albuminuria was notably higher in the high-risk group identified by AI-CXR compared to the median- and low-risk groups, with a clear dose–response relationship evident across these categories. The ability of CXRs to reflect conditions such as DM [20] and cardiac disease [24] is reasonable, as AI has previously shown efficacy in detecting systemic diseases and underlying conditions from radiographic features. This correlation between CXR findings and CKD progression is likely driven by shared pathophysiological pathways. Vascular calcifications and atherosclerosis, detectable on CXR, are established risk factors for renal decline [28]. The higher prevalence of cardiomegaly and pulmonary congestion in the high-risk group suggests volume overload and cardiovascular complications, both contributing to CKD progression. This aligns with the increased occurrence of key radiological markers, including costophrenic angle blunting, pleural effusion, atherosclerosis, cardiomegaly, prominence of hilar shadow, and inflammatory changes, in AI-CXR-identified high-risk patients. These radiological markers are closely linked to comorbid conditions like DM and cardiac disease, which are known contributors to CKD progression [11]. Therefore, it is logical that our model not only predicts CKD risk but also stratifies patients based on these established factors. This integrated risk assessment further validates the utility of our AI-CXR model, highlighting its potential as a comprehensive tool for early CKD risk stratification within standard imaging workflows.

Our findings indicate that the predictive performance of AI-CXR surpasses that of traditional risk factors combined, potentially revealing subtle features that may be challenging for human observers to detect. This phenomenon has been noted in other AI-CXR studies [29–31], where AI models have identified markers invisible to the human eye, suggesting an ability to detect early signs of systemic disease that might otherwise be overlooked. Currently, the international CKD staging criteria incorporate albuminuria because it serves as a significant predictor of CKD progression and associated adverse outcomes [32]. Elevated levels of albumin in the urine indicate kidney damage and are linked to faster declines in kidney function, increased cardiovascular events, and higher mortality rates [33]. Given the scarcity of albuminuria testing [7]—illustrated by the fact that less than 10% of patients in our sample had records of urinary protein, microalbumin, or albumin-to-creatinine ratio in the EHR—AI-CXR could potentially serve as an alternative to albuminuria for identifying early CKD. The consistency and robustness of our results lead us to have strong confidence in the potential of AI-CXR as a transformative tool in the early identification and management of CKD.

This study has several limitations. First, as a retrospective analysis, the model's performance is constrained by the quality and completeness of the available data. For example, our dataset lacked comprehensive albuminuria data, limiting the ability to directly compare the model's predictive power against established CKD biomarkers. Although the DLM using a single CXR outperformed models with additional clinical variables, this finding may be study-specific and requires validation in broader cohorts. While the model performed well in internal and external validation, its applicability to diverse populations remains uncertain due to the homogeneous study cohort from two hospitals in Taiwan. Future studies using open datasets across different regions are needed to assess generalizability. Further evidence is required to confirm the reproducibility and clinical utility of single CXR-based predictions. Finally, while our AI-CXR model successfully utilized imaging data for risk stratification, it lacks insight into causal mechanisms since the "black box" nature [34].

In conclusion, this study demonstrates that an AI-CXR model can effectively predict long-term CKD progression and associated adverse outcomes, providing a promising tool for risk stratification in clinical practice. The model can identify high-risk patients using CXR, offering a practical and accessible approach to early CKD management, especially in settings where traditional biomarkers like albuminuria may be unavailable. Importantly, individuals identified as high-risk should undergo further routine diagnostic evaluation to confirm CKD status and guide appropriate clinical management. By leveraging widely conducted imaging, the AI-CXR model could facilitate proactive CKD intervention, improving patient outcomes and contributing to more efficient resource allocation in healthcare. Further prospective validation will be essential to confirm its utility across diverse clinical environments.

Supplementary Information The online version contains supplementary material available at https://doi.org/10.1007/s10278-025-01489-4.

Author Contribution Kai-Chieh Chen, Wen-Hui Fang, Chin Lin, and Yu-Juei Hsu contributed to the study conception and design. Material preparation, data collection, and analysis were performed by Kai-Chieh Chen, Shang-Yang Lee, Dung-Jang Tsai, Kai-Hsiung Ko, Wei-Chou Chang, and Yi-Chih Hsu. The first draft of the manuscript was written by Kai-Chieh Chen and Chin Lin. Kai-Chieh Chen and Chin Lin provided a deep learning model for stratifying high risks of mortality. Kai-Chieh Chen analyzed the data. Wen-Hui Fang, Chin Lin, and Yu-Juei Hsu revised the manuscript for important intellectual content. Chin Lin and Yu-Juei Hsu took final responsibility for this article and provided the final approval of the version to be published.

Data Availability The datasets generated during and/or analyzed during the current study are not publicly available but are available from the corresponding author on reasonable request.

Declarations

Ethics Approval This study was ethically by the institutional review board (IRB NO. C202305019) in Tri-Service General Hospital, Taipei, Taiwan.

Consent to Participate Informed consent was obtained from all individual participants included in the study.

Consent for Publication My manuscript does not contain any individual person's data in any form.

Competing Interests The authors declare no competing interests.

References

1. **Global, regional, and national burden of chronic kidney disease, 1990–2017: a systematic analysis for the Global Burden of Disease Study 2017**. *Lancet (London, England)* 2020, **395**(10225):709–733.
2. Thomas R, Kanso A, Sedor JR: **Chronic kidney disease and its complications**. *Primary care* 2008, **35**(2):329–344, vii.
3. Xie X, Liu Y, Perkovic V, Li X, Ninomiya T, Hou W, Zhao N, Liu L, Lv J, Zhang H *et al*: **Renin-Angiotensin System Inhibitors and Kidney and Cardiovascular Outcomes in Patients With CKD: A Bayesian Network Meta-analysis of Randomized Clinical Trials**. *American journal of kidney diseases : the official journal of the National Kidney Foundation* 2016, **67**(5):728-741.
4. Smart NA, Dieberg G, Ladhani M, Titus T: **Early referral to specialist nephrology services for preventing the progression to end-stage kidney disease**. *The Cochrane database of systematic reviews* 2014(6):Cd007333.
5. Jha V, Garcia-Garcia G, Iseki K, Li Z, Naicker S, Plattner B, Saran R, Wang AY, Yang CW: **Chronic kidney disease: global dimension and perspectives**. *Lancet (London, England)* 2013, **382**(9888):260-272.
6. Levin A, Stevens PE: **Summary of KDIGO 2012 CKD Guideline: behind the scenes, need for guidance, and a framework for moving forward**. *Kidney international* 2014, **85**(1):49-61.
7. Benghanem Gharbi M, Elseviers M, Zamd M, Belghiti Alaoui A, Benahadi N, Trabelssi el H, Bayahia R, Ramdani B, De Broe ME: **Chronic kidney disease, hypertension, diabetes, and obesity in the adult population of Morocco: how to avoid "over"- and "under"-diagnosis of CKD**. *Kidney international* 2016, **89**(6):1363-1371.
8. Chu CD, Xia F, Du Y, Singh R, Tuot DS, Lamprea-Montealegre JA, Gualtieri R, Liao N, Kong SX, Williamson T *et al*: **Estimated Prevalence and Testing for Albuminuria in US Adults at Risk for Chronic Kidney Disease**. *JAMA network open* 2023, **6**(7):e2326230.
9. Powe NR, Boulware LE: **Population-based screening for CKD**. *American journal of kidney diseases : the official journal of the National Kidney Foundation* 2009, **53**(3 Suppl 3):S64-70.
10. Boulware LE, Jaar BG, Tarver-Carr ME, Brancati FL, Powe NR: **Screening for proteinuria in US adults: a cost-effectiveness analysis**. *Jama* 2003, **290**(23):3101-3114.
11. Shlipak MG, Tummalapalli SL, Boulware LE, Grams ME, Ix JH, Jha V, Kengne AP, Madero M, Mihaylova B, Tangri N *et al*: **The case for early identification and intervention of chronic kidney disease: conclusions from a Kidney Disease: Improving Global Outcomes (KDIGO) Controversies Conference**. *Kidney international* 2021, **99**(1):34-47.
12. Echouffo-Tcheugui JB, Kengne AP: **Risk models to predict chronic kidney disease and its progression: a systematic review**. *PLoS medicine* 2012, **9**(11):e1001344.
13. Jardine MJ, Hata J, Woodward M, Perkovic V, Ninomiya T, Arima H, Zoungas S, Cass A, Patel A, Marre M *et al*: **Prediction of kidney-related outcomes in patients with type 2 diabetes**. *American journal of kidney diseases : the official journal of the National Kidney Foundation* 2012, **60**(5):770-778.
14. Hira RS, Kennedy K, Nambi V, Jneid H, Alam M, Basra SS, Ho PM, Deswal A, Ballantyne CM, Petersen LA *et al*: **Frequency and practice-level variation in inappropriate aspirin use for the primary prevention of cardiovascular disease: insights from the National Cardiovascular Disease Registry's Practice Innovation and Clinical Excellence registry**. *Journal of the American College of Cardiology* 2015, **65**(2):111-121.
15. Vogel B, Acevedo M, Appelman Y, Bairey Merz CN, Chieffo A, Figtree GA, Guerrero M, Kunadian V, Lam CSP, Maas A *et al*: **The Lancet women and cardiovascular disease Commission: reducing the global burden by 2030**. *Lancet (London, England)* 2021, **397**(10292):2385-2438.
16. Pickhardt PJ, Summers RM, Garrett JW, Krishnaraj A, Agarwal S, Dreyer KJ, Nicola GN: **Opportunistic Screening: Radiology Scientific Expert Panel**. *Radiology* 2023, **307**(5):e222044.
17. Link TM: **Osteoporosis imaging: state of the art and advanced imaging**. *Radiology* 2012, **263**(1):3-17.
18. Tsai DJ, Lin C, Lin CS, Lee CC, Wang CH, Fang WH: **Artificial Intelligence-enabled Chest X-ray Classifies Osteoporosis and Identifies Mortality Risk**. *Journal of medical systems* 2024, **48**(1):12.
19. Lin C, Tsai DJ, Wang CC, Chao YP, Huang JW, Lin CS, Fang WH: **Osteoporotic Precise Screening Using Chest Radiography and Artificial Neural Network: The OPSCAN Randomized Controlled Trial**. *Radiology* 2024, **311**(3):e231937.
20. Pyrros A, Borstelmann SM, Mantravadi R, Zaiman Z, Thomas K, Price B, Greenstein E, Siddiqui N, Willis M, Shulhan I *et al*: **Opportunistic detection of type 2 diabetes using deep learning from frontal chest radiographs**. *Nature communications* 2023, **14**(1):4039.
21. Weiss J, Raghu VK, Paruchuri K, Zinzuwadia A, Natarajan P, Aerts H, Lu MT: **Deep Learning to Estimate Cardiovascular Risk From Chest Radiographs : A Risk Prediction Study**. *Annals of internal medicine* 2024, **177**(4):409-417.
22. Raoof S, Feigin D, Sung A, Raoof S, Irugulpati L, Rosenow EC, 3rd: **Interpretation of plain chest roentgenogram**. *Chest* 2012, **141**(2):545-558.
23. Tiu E, Talius E, Patel P, Langlotz CP, Ng AY, Rajpurkar P: **Expert-level detection of pathologies from unannotated chest**

X-ray images via self-supervised learning. *Nature biomedical engineering* 2022, **6**(12):1399-1406.
24. Ueda D, Matsumoto T, Ehara S, Yamamoto A, Walston SL, Ito A, Shimono T, Shiba M, Takeshita T, Fukuda D *et al*: **Artificial intelligence-based model to classify cardiac functions from chest radiographs: a multi-institutional, retrospective model development and validation study**. *The Lancet Digital health* 2023, **5**(8):e525-e533.
25. Chen YC, Fang WH, Lin CS, Tsai DJ, Hsiang CW, Chang CK, Ko KH, Huang GS, Lee YT, Lin C: **Integrating VAI-Assisted Quantified CXRs and Multimodal Data to Assess the Risk of Mortality**. *Journal of imaging informatics in medicine* 2024.
26. Chen YJ, Lin CS, Lin C, Tsai DJ, Fang WH, Lee CC, Wang CH, Chen SJ: **An AI-Enabled Dynamic Risk Stratification for Emergency Department Patients with ECG and CXR Integration**. *Journal of medical systems* 2023, **47**(1):81.
27. Holmstrom L, Christensen M, Yuan N, Weston Hughes J, Theurer J, Jujjavarapu M, Fatehi P, Kwan A, Sandhu RK, Ebinger J *et al*: **Deep learning-based electrocardiographic screening for chronic kidney disease**. *Commun Med (Lond)* 2023, **3**(1):73.
28. Go AS, Chertow GM, Fan D, McCulloch CE, Hsu CY: **Chronic kidney disease and the risks of death, cardiovascular events, and hospitalization**. *The New England journal of medicine* 2004, **351**(13):1296-1305.
29. Liu X, Faes L, Kale AU, Wagner SK, Fu DJ, Bruynseels A, Mahendiran T, Moraes G, Shamdas M, Kern C *et al*: **A comparison of deep learning performance against health-care professionals in detecting diseases from medical imaging: a systematic review and meta-analysis**. *The Lancet Digital health* 2019, **1**(6):e271-e297.
30. Aggarwal R, Sounderajah V, Martin G, Ting DSW, Karthikesalingam A, King D, Ashrafian H, Darzi A: **Diagnostic accuracy of deep learning in medical imaging: a systematic review and meta-analysis**. *NPJ Digit Med* 2021, **4**(1):65.
31. Rajpurkar P, Chen E, Banerjee O, Topol EJ: **AI in health and medicine**. *Nature medicine* 2022, **28**(1):31-38.
32. **KDIGO 2024 Clinical Practice Guideline for the Evaluation and Management of Chronic Kidney Disease**. *Kidney international* 2024, **105**(4s):S117-s314.
33. Pasternak M, Liu P, Quinn R, Elliott M, Harrison TG, Hemmelgarn B, Lam N, Ronksley P, Tonelli M, Ravani P: **Association of Albuminuria and Regression of Chronic Kidney Disease in Adults With Newly Diagnosed Moderate to Severe Chronic Kidney Disease**. *JAMA network open* 2022, **5**(8):e2225821.
34. LeCun Y, Bengio Y, Hinton G: **Deep learning**. *Nature* 2015, **521**(7553):436-444.